On Modelling and Control of Pantograph Catenary Systems

Simon WALTERS, Ahmed RACHID, Augustin MPANDA

***Abstract*— The paper describes modelling and control techniques studied and applied to selected pantograph-catenary (PAC) systems. The work has been co-funded by the European Union under the ERDF project: PAntograph-Catenary Interaction Framework for Intelligent Control (PACIFIC). Mechanical models of PAC systems are implemented in MATLAB using novel techniques, where applicable. Next, important physical phenomena affecting the reliability of power collection using PAC systems are considered: electrical arcing and thermal effects are both modelled. A range of control systems are then implemented within selected PAC model simulations: Linear Matrix Inequalities (LMI), and crisp and fuzzy versions of PID controllers are tested. MATLAB is used extensively. All of the PAC system and controller pairings are found to perform well in their chosen implementations, preparing the way for future extension of the PACIFIC project work into the non-linear domain using non-linear fuzzy controllers.**

I. INTRODUCTION

This paper presents completed work, and work-in-progress, undertaken as part of the EU ERDF Interreg IV project: PAntograph-Catenary Interaction Framework for Intelligent Control (PACIFIC). The work concerns the demonstration of modelling and control techniques for pantograph-catenary (PAC) systems. The paper starts by featuring finite-element and lumped-parameter models for PAC systems; the lumped-parameter models are implemented in MATLAB and incorporate embellishments for improving the realism of simulations of motion at elevated speeds. Fourth and sixth order models are presented with novel features, as applicable. Augmenting and following on from the modelling work, control systems are added to the simulation. Linear Matrix Inequalities (LMI) are implemented in conjunction with a multiple model to control a fourth order PAC system, running at constant speed. Proportional Integral Derivative (PID) and Fuzzy Proportional Derivative Plus Integral (FPD+I) controllers are then applied to a sixth order PAC model, simulating running at variable speed. The majority of the work is implemented in MATLAB and Toolboxes thereof.

A. Catenary Finite Element model

A variety of catenary models are proposed in the literature from a simple model which considers only static variation of stiffness along a span to a complete finite element model (FEM) which describes more accurately the non-linear dynamic interaction of pantograph-catenary. High accuracy models are required especially for in the high-speed range where the wave reflection becomes a major cause of contact loss [1].

Moreover, the effect of other elements such as brackets, registration arms and droppers should be taken into consideration (Fig. 1). The common mathematical model that can be used for the messenger and contact wires is [1], [2] :

$$\rho_A \frac{\partial^2 z(x,t)}{\partial t^2} + c\frac{\partial z(x,t)}{\partial t} - T\frac{\partial^2 z(x,t)}{\partial x^2} = q(x,t)$$

which describes the wire as an homogenous string mass per unit length ρ_A with tensile force T and viscous damping determined by the parameter. The function $q(x,t)$ represents the force distribution on the string and parameter z represents the vertical displacement from equilibrium profile. The beam models (Euler-Bernoulli-Timoshenko beam) give more accurate results as discussed in [3]. The Euler-Bernoulli beam model takes the bending stiffness of the wire into account and, in addition, the Timoshenko beam model considers the effects of shear deformation and rotary inertia. The equation of two-node Euler-Bernoulli-Timoshenko beam is given by:

$$\rho_A \frac{\partial^2 z(x,t)}{\partial t^2} + c\frac{\partial z(x,t)}{\partial t} + EI\frac{\partial^4 z(x,t)}{\partial t^4} - T\frac{\partial^2 z(x,t)}{\partial X^2} = q(x,t)$$

where EI (E is the Young modulus and I is the moment of inertia) denotes the flexural rigidity of the wire. For the messenger wire only, the effects of droppers and brackets are presented in $q_m(x,t)$ function by:

$$q_m(x,t) = \sum_{j=1}^{n\circ\text{drop}} f_{dr,i}(t)\delta(x-x_j) - \sum_{k=1}^{n\circ\text{brk}} f_{br,k}(t)\delta(x-x_k)$$

where $f_{br,k}(t)$ is the external forces by $n\circ$brk brackets which are located in x_k, $f_{dr,i}(t)$ represent the external force by $n\circ$drop droppers which are located in x_i and $\delta(t)$ represents Dirac delta function $at x = 0$. The contact wire is subjected to the external forces on the registration arms $f_{re,j}(t)$ instead of external forces on the brackets $f_{br,k}(t)$ and the contact force represented by $f_c(t)$, hence the function $q_c(x,t)$ can be

This work is part-financed by the ERDF as part of the INTERREG IV A France (Channel) England cross-border European cooperation programme.

Ahmed RACHID is a Professor at the University of Picardie Jules Verne, 33 rue Saint LEU. 80000 Amiens, France. rachid@u-picardie.fr

Augustin MPANDA is an Associate Professor at ESIEE-Amiens, Amiens, France. mpanda@esiee-amiens.fr

Simon WALTERS is a Senior Lecturer at the University of Brighton, Brighton, U.K. s.d.walters@brighton.ac.uk

written as:

$$q_c(x,t) = f_c(t)\delta(x-Vt) - \sum_{j=1}^{n} \circ \mathrm{drop} f_{dr,i}(t)\delta(x-x_j) - \sum_{j=1}^{n} reg f_{re,j}(t)\delta(x-x_j)$$

Brackets are really stiff constraints that can be considered as fixed points. This component has been modelled as spring-damper system with high stiffness coefficient, and zero damping and masses.

$$f_{bri} = c_{br,i} \cdot \dot{z} + kbr, i \cdot z$$

where: f_{bri}, c_{bri} and k_{bri} are the i^{th} bracket force, damping and stiffness respectively. Like the brackets, even the registration arms can be modelled as a complete spring damper mass system.

$$f_{regi} = m_{regi} \cdot \ddot{z} + c_{regi} \cdot \dot{z} + k_{regi} \cdot z + m_{regi} \cdot g$$

where f_{regi}, m_{regi}, c_{regi}, k_{regi} are i^{th} registration arm force, mass, damping and stiffness respectively. Droppers, in order to achieve a more general formulation of the problem, are modelled with the spring-damper-mass scheme so:

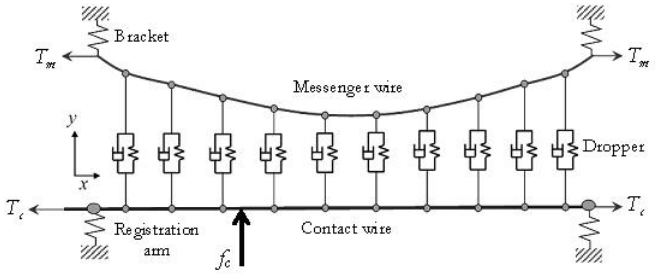

Model of catenary system represents the mass summed for half of the dropper and its clamp represents the mass of registration arm

$$f_{dri} \cdot (\ddot{z}_{mi} - \ddot{z}_{ci}) + c_{dri} \cdot (\dot{z}_{mi} - \dot{z}_{ci}) + k_{dri} \cdot (z_{mi} - z_{ci}) + f_{dro} + m_{dri} \cdot g$$

where: f_{dri}, m_{dri}, c_{dri}, k_{dri} are i^{th} dropper force, mass, damping and stiffness respectively and $z_{m_i}$and z_{ci} are vertical displacement between messenger and catenary wires at i^{th} dropper position. The above model can be extended in 3D considering the horizontal displacement of contact wire as it is presented in [4], [5].

II. PAC MODELLING

A. PAC 4th order model

The pantograph is shown in Figure 1 and it is represented by the 2 degrees of freedom mechanical system in Figure 2. The catenary is generally represented by a time-variant stifness $k(t)$ as in [6].

The state space representation of the PAC system is [7]:

$$\begin{cases} \dot{z}(t) &= A(t)z(t) + Bu(t) \\ y(t) &= C(t)z(t) \end{cases} \quad (1)$$

where

$$z = \begin{bmatrix} z_1 & z_2 & z_3 & z_4 \end{bmatrix}^T = \begin{bmatrix} x_1 & \dot{x}_1 & x_2 & \dot{x}_2 \end{bmatrix}^T$$

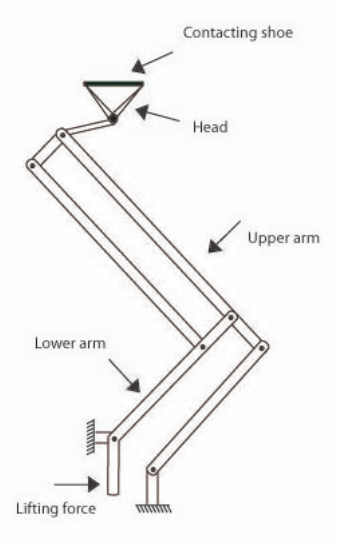

Fig. 1. Pantograph mechanism

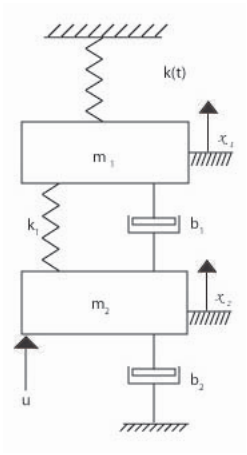

Fig. 2. The pantograph 4th order model

$$A(t) = \begin{bmatrix} 0 & 1 & 0 & 0 \\ -\frac{k_1 + k(t)}{m_1} & -\frac{b_1}{m_1} & \frac{k_1}{m_1} & \frac{b_1}{m_1} \\ 0 & 0 & 0 & 1 \\ \frac{k_1}{m_2} & \frac{b_1}{m_2} & -\frac{k_1}{m_2} & -\frac{b_1 + b_2}{m_2} \end{bmatrix},$$

$$B = \begin{bmatrix} 0 & 0 & 0 & \frac{1}{m_2} \end{bmatrix}^T, \quad C(t) = \begin{bmatrix} k(t) & 0 & 0 & 0 \end{bmatrix},$$

with (see [6]):

$$k(t) = K_0 \left(1 + \alpha \cos\left(\frac{2\pi V}{L} t \right) \right) \quad (2)$$

V is the train speed (m/s); L the span length (m); K_0 the average equivalent stiffness (N/m); α is the stiffness variation coefficient in a span. Typical values of the model parameters are given in Table 1. We also have ([6])

$$\alpha = \frac{K_{\max} - K_{\min}}{K_{\max} + K_{\min}}, \qquad K_0 = \frac{K_{\max} + K_{\min}}{2}$$

$K_{\max}$, $K_{\min}$ being the maximum and minimum stiffness value in a span (N/m), respectively.

B. PAC 6th order model

In this section, the PAC system is represented by the 3 degree of freedom mechanical system in Figure 3.

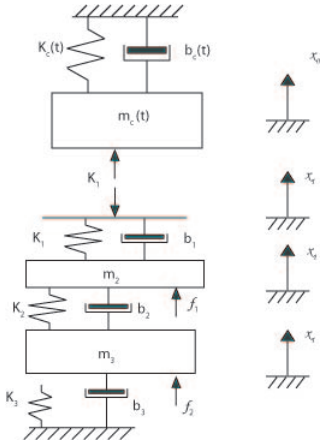

Fig. 3. PAC 6th order model

The state space representation of the PAC system is:

$$\begin{cases} \dot{x} = A(t)x + B_c f_c + B_q f_q \\ y = Cx \end{cases} \tag{3}$$

where

$$\begin{aligned} x &= \begin{bmatrix} x_1 & x_2 & x_3 & x_4 & x_5 & x_6 \end{bmatrix}^T \\ &= \begin{bmatrix} x_1 & \dot{x}_1 & x_2 & \dot{x}_2 & x_3 & \dot{x}_3 \end{bmatrix}^T \end{aligned}$$

$$A(t) = \begin{bmatrix} 0 & 1 & 0 & 0 & 0 & 0 \\ -\frac{k_1+k_c(t)}{m_c(t)} & -\frac{b_1+b_c(t)}{m_c(t)} & \frac{k_1}{m_c(t)} & \frac{b_1}{m_c(t)} & 0 & 0 \\ 0 & 0 & 0 & 1 & 0 & 0 \\ \frac{k_1}{m_2} & \frac{b_1}{m_2} & a_{33} & a_{34} & \frac{k_2}{m_2} & \frac{b_2}{m_2} \\ 0 & 0 & 0 & 0 & 0 & 1 \\ 0 & 0 & \frac{k_2}{m_3} & \frac{b_2}{m_3} & a_{65} & a_{66} \end{bmatrix}$$

with

$$a_{33} = -\frac{k_1+k_2}{m_2}, \qquad a_{34} = -\frac{b_1+b_2}{m_2}$$

$$a_{65} = -\frac{k_2+k_3}{m_3} \qquad a_{66} = -\frac{b_2+b_3}{m_3}$$

$$\begin{aligned} B_c &= \begin{bmatrix} 0 & 0 & 0 & \frac{1}{m_2} & 0 & 0 \end{bmatrix}^T \\ B_q &= \begin{bmatrix} 0 & 0 & 0 & 0 & 0 & \frac{1}{m_3} \end{bmatrix}^T \\ C &= \begin{bmatrix} -k_1 & -b_1 & k_1 & b_1 & 0 & 0 \end{bmatrix}. \end{aligned}$$

The catenary parameters present a periodic behaviour varying along each span, with small variations due to the droppers. This can be represented by a combination of harmonic functions ([2])

$$\begin{aligned} m_c(t) &= m_{c0} + \textstyle\sum_{i=1}^{3} m_{ci} \cos(\frac{2i\pi}{L} x(t)) \\ b_c(t) &= b_{c0} + \textstyle\sum_{i=1}^{3} b_{ci} \cos(\frac{2i\pi}{L} x(t)) \\ k_c(t) &= k_{c0} + \textstyle\sum_{i=1}^{3} k_{ci} \cos(\frac{2i\pi}{L} x(t)) \end{aligned}$$

III. PAC Physical phenomena

A. Pantograph arcing

Pantograph-catenary contact losses and overhead line thermal effect have been studied within the framework of the PACIFIC project. The loss of contact between the pantograph and the catenary creates an electric flash (electric arc) which accelerates the degradation of both the contact strips on the bow and the contact wire resulting in a poor energy quality factor. Also as a consequence of contact losses, the pantograph arcing generates the EMC problems. Arcing distorts the current and voltage waveforms during the current zero crossing (CZC). The Figure 4, below, [8] represents 3 modes of contact losses:

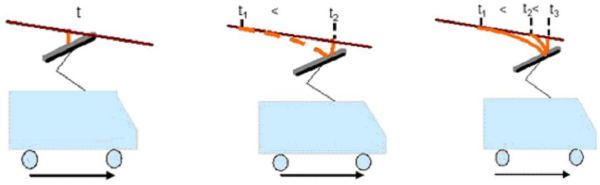

Fig. 4. 3 possible modes of contacts sliding contacts during pantograph arcing

- Mode 1: The arc root can glide continuously along the contact wire. This would happen when the pantograph and the contact wire are firmly connected or the train is moving at a very slow speed.
- Mode 2: The arc root can hop in smaller lengths down the contact wire. The voltage will have either smaller overshoots or notches just after the CZC.
- Mode 3: The arc root elongates to a long length. This can happen with high current and high speed either at every CZC.

To take account of the pantograph arcing, these 3 modes have been implemented in the pantograph-catenary interaction simulation programme using a circuit breaker represented by the Mayr arc model, as shown in Figure 5.

The Mayr model is applied for the approximation of the electric arc behaviour in the range of the CZC. It is a function of the arc conductance. The arc is described by the rate of

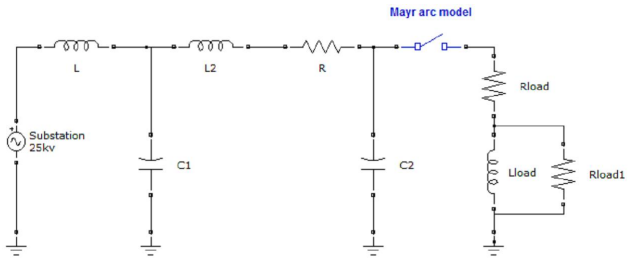

Fig. 5. Electric model of the pantograph-catenary interaction

change of the conductance with the arc current and voltage. The Mayr arc model is described by the following equation [9]:

$$\frac{1}{g}\frac{dg}{dt} = \frac{d\ln g}{dt} = \frac{1}{\tau}\left(\frac{ui}{P} - 1\right)$$

where:
g: the dynamic conductance of the electric arc column (supposed to have an exponential variation versus the stored energy,
u: instantaneous value of the arc voltage,
τ: time constant of the electric arc at the 'current zero' moment,
U_c: the electric arc voltage, considered to be constant.

The simulation results for voltage and current waveforms for the 3 modes are given in Figures 6 to 8 below.

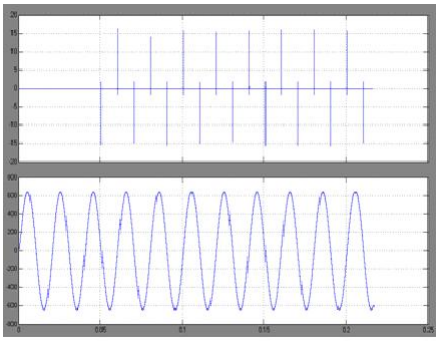

Fig. 6. Voltage (V) (upper) and current (A) waveforms for 1stF Mode

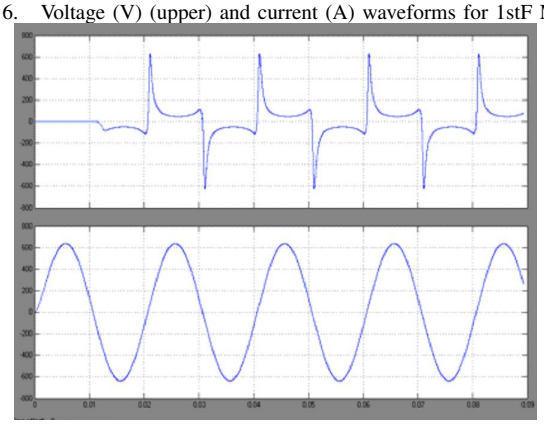

Fig. 7. Voltage (V) (upper) and current (A) waveforms for 2nd Mode

During the first mode, it can be seen that the arc current waveform is sinusoidal and at the CZC, there is a peak

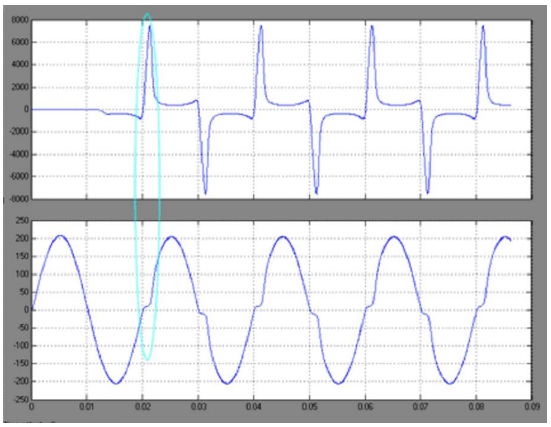

Fig. 8. Arc voltage (V) and current (A) waveforms for 3 rd Mode

of the arc voltage. For the second mode, Figure 7 shows that at each CZC the voltage signal has either overshoots or notches. In Figure 8, it can be observed that during the short period the current is zero, there is an overshoot on the arc voltage. All these results are in accordance with the experimentation in [8]. In Figure 9, the simulation is related to 2 arcs appearing consecutively. Within the Pacific test bench, further investigation and experimentation are expected to confirm the arc modelling.

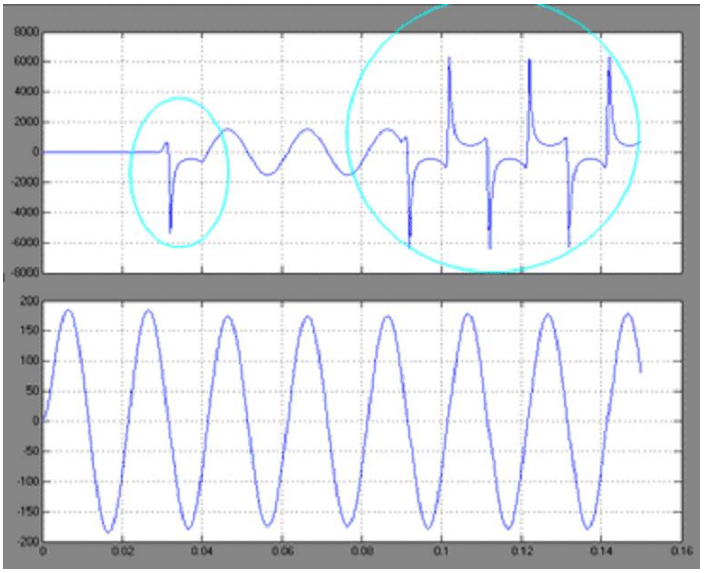

Fig. 9. Arc voltage (V) and current (A) waveforms for repetitive arcing

B. Thermal effects

The contact occurring between contact strip and contact wire is mostly influenced by the dissipated power at the contact. In the case of electromechanical contact under study, the dissipated power is due to arcing, friction effect and Joule effect. Neglecting the arcing effect, it is proposed according to [10], to estimate the heat flow per unit area, q, as:

$$q = \frac{\mu P v}{A_n} + \frac{R_{el,c} I^2}{A_n}$$

The electrical contribution is assumed as a normal force $P_{eq,el} = R_{el,c}I^2/(\mu v)$, P being normal force on sliding interface between the 2 bodies, the friction coefficient, v the sliding speed and I the current flow intensity.

Based on this theory, the model established with 2D Comsol Multi-PFhysics allows the evaluation of the thermal contact between the contact strip and the contact line (Figure 10) whereas the temperature change is given in Figure 11 within 3000s of contact duration.

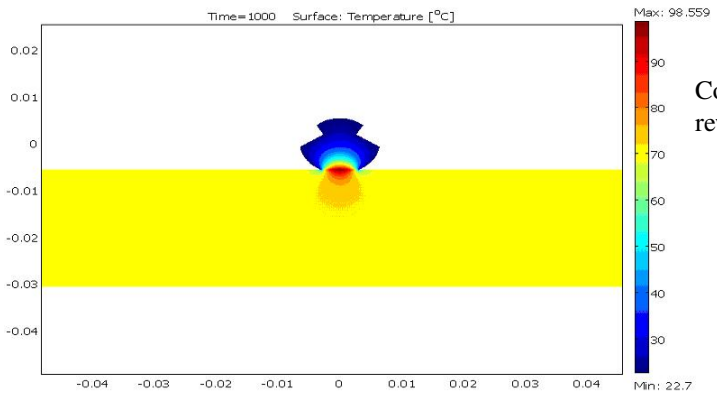

Fig. 10. Temperature distribution in the contact line/contact strip system

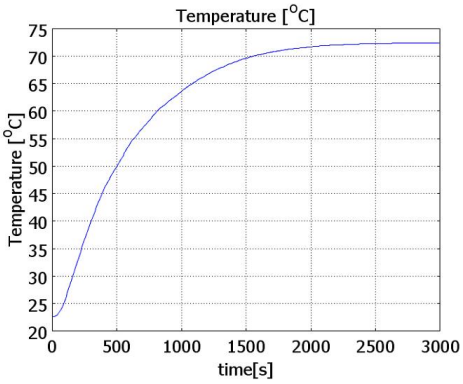

Fig. 11. Temperature as time function for the contact strip

For the copper based contact strip with: $\mu = 0.76$, I =750 A, V = 70 m/s, $Rc = 0.008\Omega$. Under the normal force N = 100 N, $Tmax$ is equal to 99°C with the friction and Joule powers estimated at 5320 W and 4500 W respectively; larger than the Joule effect in this case. It can be concluded that in this particular case of a copper contact strip, mechanical and electrical parameters (speed, normal force, friction coefficient and current) are the essential parameters governing the heat transfer.

IV. LMI Control and Observation

A. LMI PAC Control

In this section, LMIs (Linear Matrix Inequalities) are used to control the PAC system modelled by the multiple model (3). LMIs have been extensively used in control theory [22] due to their simple formulation and available computing solvers such as the LMI MATLAB Toolbox.

A multiple mode is derived for instance for the 4th order model case. To this end, it can be seen from (2) that $k(t)$ can be bounded as

$$\underline{K} = K_0(1-\alpha) \leq k(t) \leq \overline{K} = K_0(1+\alpha)$$

inducing

$$-\frac{k_1+\overline{K}}{m_1} \leq -\frac{k_1+k(t)}{m_1} \leq -\frac{k_1+\underline{K}}{m_1}$$

Consequently, the PAC state space system model (1) can be rewritten in terms of a multiple model, that is

$$\begin{cases} \dot{z} &= (\mu_1 A_1 + \mu_2 A_2)z + Bu \\ y &= (\mu_1 C_1 + \mu_2 C_2)z \end{cases} \tag{4}$$

where $\mu_1 + \mu_2 = 1$, and

$$\mu_1 = \frac{\overline{K} - k(t)}{\overline{K} - \underline{K}} \geq 0, \qquad \mu_2 = \frac{k(t) - \underline{K}}{\overline{K} - \underline{K}} \geq 0$$

$$\begin{cases} A_1 = \begin{bmatrix} 0 & 1 & 0 & 0 \\ -\frac{k_1+\overline{K}}{m_1} & -\frac{b_1}{m_1} & \frac{k_1}{m_1} & \frac{b_1}{m_1} \\ 0 & 0 & 0 & 1 \\ \frac{k_1}{m_2} & \frac{b_1}{m_2} & -\frac{k_1}{m_2} & -\frac{b_1+b_2}{m_2} \end{bmatrix} \\ C_1 = \begin{bmatrix} \underline{K} & 0 & 0 & 0 \end{bmatrix} \\ A_2 = \begin{bmatrix} 0 & 1 & 0 & 0 \\ -\frac{k_1+\underline{K}}{m_1} & -\frac{b_1}{m_1} & \frac{k_1}{m_1} & \frac{b_1}{m_1} \\ 0 & 0 & 0 & 1 \\ \frac{k_1}{m_2} & \frac{b_1}{m_2} & -\frac{k_1}{m_2} & -\frac{b_1+b_2}{m_2} \end{bmatrix} \\ C_2 = \begin{bmatrix} \overline{K} & 0 & 0 & 0 \end{bmatrix} \end{cases} \tag{5}$$

Now considering the PAC system described by (3), the control objective is to drive the output contact force $y(t)$ to a desired constant y_d, the typicaly desired value being $y_d = 100$ N.

To this end, an integrator is introduced

$$w(t) = \int_0^t (y_d - y(\theta))\theta$$

or equivalently:

$$\dot{w}(t) = y_d - y(t) \tag{6}$$

This ensures a zero steady state error. Indeed, at the steady state where $\dot{w}(t) = 0$, $y(t) = y_d$ is obtained due to equation (8).

Combining this equation with the system dynamics (3) yields:

$$\begin{cases} \dot{z} & = (\mu_1 A_1 + \mu_2 A_2) z + Bu \\ y & = (\mu_1 C_1 + \mu_2 C_2) z \\ \dot{w}(t) & = y_d - y(t) = -\mu_1 C_1 - \mu_2 C_2 + y_d \end{cases}$$

which can be written more compactly under the augmented state space representation:

$$\dot{z^a} = (\mu_1 F_1 + \mu_2 F_2) z^a + Gu + M y_d \tag{7}$$

where

$$z^a = \begin{bmatrix} z \\ w \end{bmatrix},\ F_i = \begin{bmatrix} A_i & 0_{4\times 1} \\ -C_i & 0 \end{bmatrix},\ G = \begin{bmatrix} B \\ 0 \end{bmatrix},\ M = \begin{bmatrix} 0_{4\times 1} \\ 1 \end{bmatrix}.$$

Next, the control law $u = -Fz^a$ with $F = (1/2)G^T X^{-1}$ is applied, X being the positive definite solution of the LMIs.

$$\begin{cases} F_1 X + X F_1^T - GG^T < 0 \\ F_2 X + X F_2^T - GG^T < 0 \end{cases} \tag{8}$$

B. LMI PAC Observer

The augmented system $\{F_i, H_i\}$ with $H_i = \begin{bmatrix} C_i & 0 \end{bmatrix}$ is not observable, whereas $\{A_i, C_i\}$, $i = 1,2$, is. Hence an observer is assumed for the state vector z, the last state variable w of z^a can be estimated by a direct calculation from its dynamic equation (8), *i.e.* $\dot{w}(t) = y_d - y(t)$, $y(t)$ being the measured output at time t.

Therefore the observer has the form

$$\begin{cases} \dot{\hat{z}} = (\mu_1 A_1 + \mu_2 A_2)\hat{z} + Gu + (\mu_1 L_1 + \mu_2 L_2)(y - \hat{y}) \\ \hat{y} = (\mu_1 C_1 + \mu_2 C_2)\hat{z} \end{cases} \tag{9}$$

where: $L_i = (1/2)X^{-1}C_i^T$, i=1,2; X is a positive definite matrix satisfying the LMIs

$$\begin{cases} A_i^T X + X A_i - C_i^T C_i < 0, \quad i = 1,2 \\ X > 0 \end{cases} \tag{10}$$

This dynamics should be combined with the integrator equation (8) in order to get the overall augmented state z^a in (9).

C. LMI Simulation

Using the MATLAB LMI toolbox, conditions (10) with $\alpha = 10$ and $\beta = 50$ for the controller and (12) for the observer have been proven to be feasible with the parameters given in [7] and reproduced in Table 1. In Figure 12, the obtained contact force can be seen corresponding to a desired value of 100 N. Figures 13 to 16 illustrate the resulting state space variables as defined for system (1). These plots clearly show satisfactory behaviour and highlight the feasibility of the proposed methods.

However, it should be noted that the results correspond to a specified constant speed V and are only valid for the chosen speed.

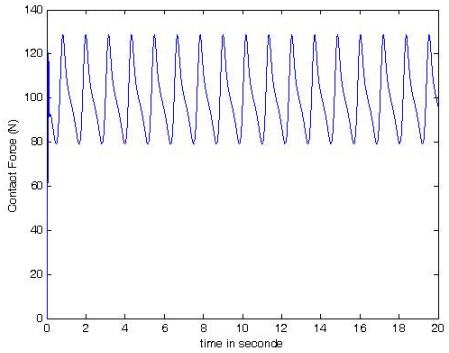

Fig. 12. The contact force

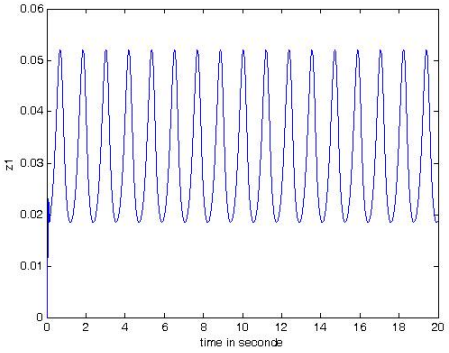

Fig. 13. The pantograph head displacement x_1

V. Fuzzy Control

A. Mechanical System Model

A sixth-order model of a PAC system has been constructed in MATLAB, as per section II.B of this paper, drawing on previous work in the PAC modelling arena; [24], [25]. This relatively high-order model was chosen for its ability to express in detail interactions between the pantograph and the catenary, without recourse to more complex finite-element implementations. Variable parameter values are also available for this type of model. One of the primary advantages of the chosen sixth-order physical model is that a good assessment of the effect of train speed on the catenary may be made; this is of critical importance when simulating high-speed trains and their special problems of power collection. The time-varying expressions for adding speed to the model were of the form considered in section II.B of this paper; time-varying parameters for the catenary: mass, stiffness and damping were included. The system was expressed as a system of differential equations and solved as a simulation of the closed-loop system indicated in Figure 17.

Initially, the model was simulated in open-loop mode, which confirmed that it was behaving as expected. After this, closed-loop assessments were made, using appropriate control algorithms. A systematic design process for fuzzy logic control systems has been published in [26], offering

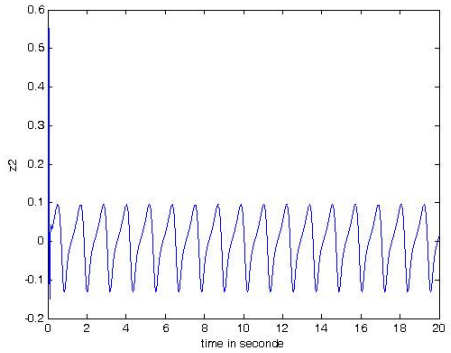

Fig. 14. The head speed $\dot{x}_1$

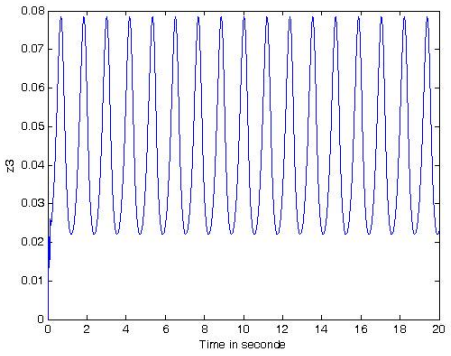

Fig. 15. The frame displacement x_2

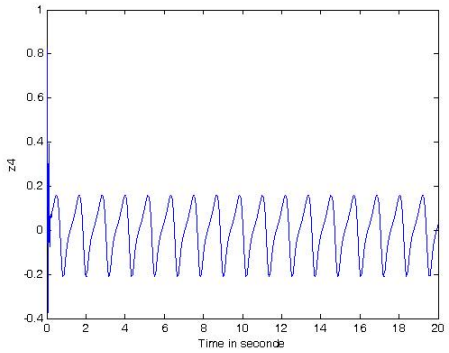

Fig. 16. The frame speed $\dot{x}_2$

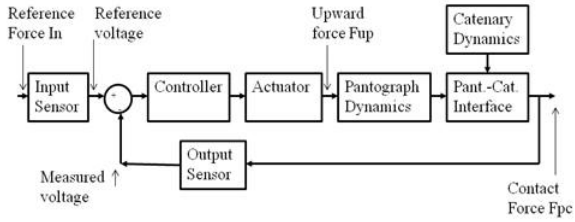

Fig. 17. Arrangement of the Control System for a PAC System

the potential for a high probability of robustness. The recommended process is as follows:

1) A conventional (crisp) PID controller is built and tuned using established techniques first.
2) Next, the crisp PID controller is replaced with an equivalent linear fuzzy controller.
3) The next stage offers a real chance to exploit the benefits of fuzzy control through the addition of non-linearity.
4) Finally, the controller is fine-tuned, before introduction to the target real-life application.

With reference to this design process, a PID controller algorithm was added to the model in question first.

B. PID Control

For the purpose of this work, the following discrete approximation for crisp PID control was used:

$$u(n) = K_p\big(e(n) + \frac{1}{T_i}\Sigma_{j=1}^{n} e(j)T_s + T_d\frac{e(n)-e(n-1)}{T_s}\big)$$

Attempts were made to derive the adjustable parameters (K_p, T_i and T_d) of the PID controller using Ziegler-Nichols frequency response tuning method. These efforts were frustrated by the margin of operation being rather narrow between under- and over-shoot. Finally, reasonable results were obtained using hand-tuning techniques described in [26] and [27].

C. Fuzzy PID Control

A linear fuzzy controller was built around the mechanical system model, for comparison with, and development from, the PID controller. A single-input, single output fuzzy system is shown in Figure 18. This is similar to the control techniques used in this work, since the derivative and integral of the error signal were derived inside the controller from the error signal. It will be noted that there is potentially somewhat greater complexity in implementing the fuzzy logic system, compared with the PID controller.

An approximation to fuzzy PID control, the Fuzzy PD+I controller in [26], was used, as shown in Figure 19. This implementation uses a control surface representing the P and D parameters, in combination with a conventional integrator. There are more gain parameters to set in the FD+I fuzzy controller, compared with the PID controller (Error gain GE, change in error gain GCE, integral of error gain GIE, and output gain GU); these ensure that the error e and change in error ce inputs and the u output are scaled as accurately as possible, to match the control surface and rule ranges.

The implementation of the PD section of the linear FPD+I controller was as shown in Figure 20. The combination of linear membership functions and effectively a summation arising from the resulting flat control surface gives a linear control system.

Comparative test runs were arranged using the PID and FPD+I controllers. An example of a simulation is given in

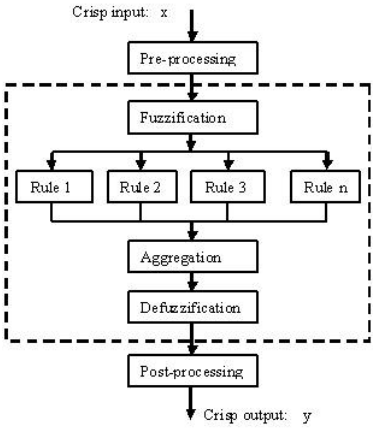

Fig. 18. Single-input Single-output Fuzzy Controller ([28])

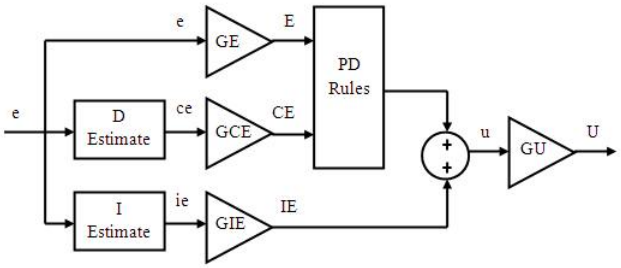

Fig. 19. FPD+I Controller ([26])

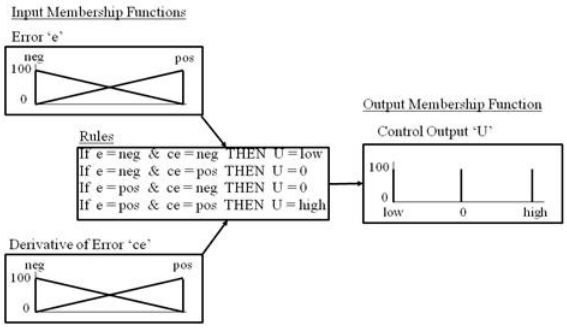

Fig. 20. A Four-rule Example of Implementation of the linear PD Controller

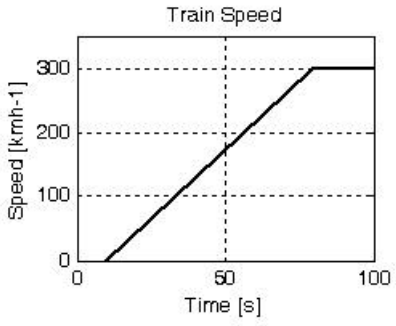

Fig. 21. Profile of train speed for test simulation

Figure 21, in which a train was to remain stationary until time t = 10 seconds before accelerating linearly to 300km/h and then from t = 80 seconds onwards, hold this speed.

D. Results

Plots of Control Force and resulting Contact Force are shown for a reference contact force of 100 N; the initial two seconds of the waveforms are shown expanded for clarity. It will be noted from Figures 22 and 23 that the PID and FPD+I results are similar, as should be the case for this linear comparison example. For both controllers, there is a degree of high frequency noise that could perhaps be filtered, yielding better performance.

VI. Conclusion

MATLAB code has been written, modelling a sixth-order pantograph-catenary (PAC) rail power collection system in connection with crisp and fuzzy PID-type controllers. Initial simulation results have been given for a train undergoing an acceleration cycle from 0 - 300 km/h. The results were found to be reasonable and similar for both controllers, during this initial comparison test. However, the inherently complex nature of the PAC system led to difficulty with tuning these linear controllers.

The Interreg-funded PACIFIC project is enabling several novel approaches to PAC modelling and control to be tested. MATLAB has been used to implement various mechanical models of PAC systems and components thereof. A multiple model has been combined with the LMI control technique to produce a new control demonstration. A range of crisp and fuzzy controllers is being evaluated and a comparison of PID and fuzzy PID controllers has been demonstrated. Electric arc and thermal models have been successfully developed

TABLE I
PAC PARAMETERS

Parametres	Notations	Value
Catenary	K_0	3.6 kNm^{-1}
	α	0.5
	L	65 m
Pantograph head	m_1	8 kg
	b_1	120 N sm^{-1}
	k_1	10 kNm^{-1}
Pantograph frame	m_2	12 kg
	b_2	30 N sm^{-1}

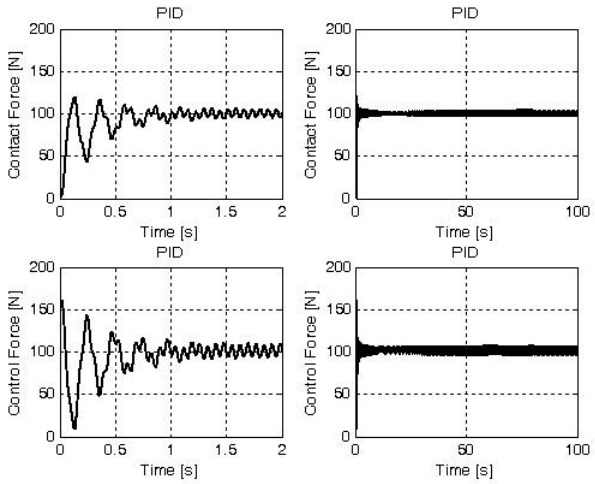

Fig. 22. PID Controller Results

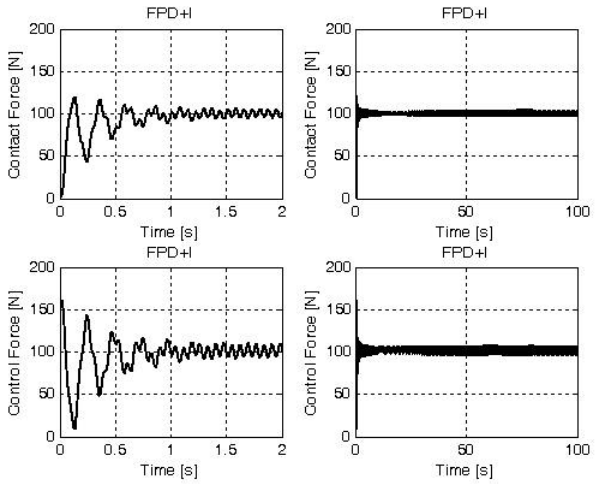

Fig. 23. FPD+I Controller Results

and applied to demonstrate physical phenomena in PAC systems.

Future work is concentrating on improving the performance of the fuzzy controller through exploiting the opportunities of non-linearity. Experiments will also be extended to cover other fuzzy control paradigms.

REFERENCES

[1] Allotta B., L. Pugi, F. Bartolini, Design and experimental results of an active suspension system for a high-speed pantograph, *IEEE Transactions on Mechatronics*, vol. 13, no. 5, pp. 548-557, 2008.

[2] Balestrino A. & al., "Innovative Solutions for Overhead Catenary-Pantograph System: Wire Actuated Control and Observed Contact Force", *Vehicle System Dynamics, vol 33, 2000, pp. 69-89.*

[3] Allotta B. & al., Experimental campaign on a servo-actuated pantograph, in *Proc. of IEEE/ASME International Conference on Advanced Intelligent Mechatronics*, Como (Italy), 8-12 Jul. 2001, pp. 237-242.

[4] Y.-C. Lin et al. Robust active vibration control for rail vehicle pantograph, *IEEE Transaction on Vehicular Technology*, vol. 56, no. 4, pp. 1994-2004, 2007.

[5] F. Resta, A. Collina, F. Fossatti, Actively controlled pantograph: an application, in *Proc. of IEEE/ASME International Conference on Advanced Intelligent Mechatronics*, Como (Italy), 8-12 Jul. 2001, pp. 243-248.

[6] Wu T.X., Brennan M.J., "Active Vibration Control of a Railway Pantograph", *in Proc. Instn Mech Engrs,. 211 (F)*, pp. 117-130, 1997.

[7] O'Connor N.D., Eppinger S.D., Seering W.P., Wormley D.N., "Active Control of a High speed Pantograph", *J. of Dynamic Systems, Measurement, and Control*, vol. 119, 1997.

[8] Midya S., D. Bormann, A. Larsson, T. Schtte, and R. Thottappillil, Understanding pantograph arcing in electrified railways influence of various parameters, *Proceedings of IEEE International Symposium on Electromagnetic Compatibility*, Detroit, Michigan, USA, Aug. 2008

[9] P.H. Schavemaker, L. Van Der Sluis. 2002. "An improved Mayr-type arc model based on current-zero measurements." *IEEE Transactions on Power delivery*, 15(2), 580-584.

[10] G. Bucca, A. Collina, "A procedure for the wear prediction of collector strip and contact wire in pantograph-catenary system", *Elsevier, Wear* 266 1-2 (2009): 46-59

[11] Eppinger S.D., O'Connor N.D., Seering W.P., Wormley D.N., "Modeling and Experimental Evaluation of Assymetric Pantograph Dynamics", *J. of Dynamic Systems, Measurement, and Control - Trans. ASME*, 110, pp.168-174, 1988.

[12] Poetsch G., Evans J., Meisinger R., Kortum W., Baldauf W., Veitl A., Wallaschek J., "Pantograph/Catenary Dynamics and Control", *Vehicle System Dynamics*, 28, pp. 159-195, 1997.

[13] Collina A. & Stefano Bruni, "Numerical Simulation of Pantograph-Overhead Equipment Interaction", *Vehicle System Dynamics*, 2002, Vol. 38, No. 4, pp. 261291.

[14] Arnold M., Simeon B., Pantograph and catenary dynamics: a benchmark problem and its numerical solution, *Journal of Applied numerical mathematics*, vol. 34, no. 4, pp. 345-362, 2000.

[15] Grases Rauter F. et al., 'Contact Model for the Pantograph-Catenery Interaction", *Journal of System Design and Dynamics*, Vol 3, N 3, 2007.

[16] M. Schaub, B. Simeon, Pantograph-catenary dynamics: an analysis of models and simulation techniques, *Journal of Mathematical and Computer Modelling of Dynamical Systems*, vol. 7, no. 2, pp. 225-238, Jun. 2001.

[17] Benet Jesus & al. A Mathematical Model of the Pantograph-Catenary Dynamic Interaction with Several Contact Wires *IAENG International Journal of Applied Mathematics*, 37:2, IJAM, 37, 2, 10.

[18] Metrikine A.V., A.L. Bosch., "Dynamic response of a two-level catenary to a moving load", *Journal of Sound and Vibration*, 292 (2006) 676-693.

[19] Zhang W., Y. Liu, G. Mei, Evaluation of the coupled dynamical response of a pantograph-catenary system: contact force and stresses, *Journal of Vehicle System Dynamics*, vol. 44, no. 8, pp. 645-658, Aug. 2006.

[20] Sergeev A. D., "Nonlinear Interaction of the Pantograph of Electric Rolling Stock and the Overhead Catenary Suspension System", *Journal of Machinery Manufacture and Reliability, 2007,* Vol. 36, No. 2, pp. 178-184.

[21] Arias E. & al., A mathematical model of the static pantograph-catenary interaction, *International Journal of Computer Mathematics*, vol. 86, no. 2, pp. 333-340, Feb. 2009.

[22] VanAntwerp J.G., D. Braatz R.D., "A tutorial on linear and bilinear matrix inequalities", *Journal of Process Control*, vol. 10, 2000, p. 363-385.

[23] Takagi T., M. Sugeno, "Fuzzy identification systems and its applications to modeling and control". *IEEE Trans. Syst. Man Cybern.*, vol. 15, 1985, p. 116-132.

[24] Hedayati S. Kia et al., Pantograph-catenary interaction model comparison, in Proc. of IEEE IECON, Arizona (USA), 7-10 Nov. 2010, pp. 1578-1583.

[25] A. Pisano, E. Usai, "Contact Force Regulation in Wire-actuated Pantographs". *Modern Sliding Mode Control Theory*, vol. 375, 2008, pp. 447-463.

[26] Jantzen Jan Foundations of Fuzzy Control, *Technical University of Denmark, John Wiley and Sons Ltd.*, 2007.

[27] Atherton D., "Control Engineering", *Ventus Publishing ApS, Boon-Books*, 2009.

[28] Lee S. H., R. J. Howlett, C. Crua, S. D. Walters, "Fuzzy Logic and Neuro-fuzzy Modelling of Diesel Spray Penetration: A Comparative Study, *Journal of Intelligent and Fuzzy Systems*, ISSN: 1064-1246 vol 18, no 1, 2007, pp 43-56.